Enhanced Vertical Charge Transport of Homo- and Blended Semiconducting Polymers by Nanoconfinement

Jongkuk Ko, Youngkeol Kim, Jin Soo Kang, Rüdiger Berger,* Hyunsik Yoon,* and Kookheon Char*

The morphology of conjugated polymers has critical influences on electronic and optical properties of optoelectronic devices. Even though lots of techniques and methods are suggested to control the morphology of polymers, very few studies have been performed inducing high charge transport along out-of-plane direction. In this study, the self-assembly of homo- and blended conjugated polymers which are confined in nanostructures is utilized. The resulting structures lead to high charge mobility along vertical direction for both homo- and blended conjugated polymers. Both semicrystalline and amorphous polymers show highly increased population of face-on crystallite despite intrinsic crystallinity of polymers. They result in more than two orders of magnitude enhanced charge mobility along vertical direction revealed by nanoscale conductive scanning force microscopy and macroscale IV characteristic measurements. Moreover, blends of semicrystalline and amorphous polymers, which are known to show inferior optical and electrical properties due to their structural incompatibility, are formed into harmonious states by this approach. Assembly of blends of semicrystalline and amorphous polymers under nanoconfinement shows charge mobility in out-of-plane direction of 0.73 cm^2 V^{-1} s^{-1} with wide range of absorption wavelength from 300 to 750 nm demonstrating the synergistic effects of two different polymers.

Development of organic electronics was led by synthesizing new materials having various electrical, optical, and structural properties from the polythiophenes to donor–acceptor monomer based low bandgap polymers. Polythiophens,[1–7] most widely studied materials, have shown enormous possibilities and various application due to their ease of processing and relatively higher charge mobility based on their semicrystalline properties. However, they suffer from low device performances

and limited applications because of relatively large optical bandgaps and moderate level of charge mobility. Low bandgap polymers[8–13] based on donor–acceptor monomers, such as poly([2,6′-4,8-di(5-ethylhexylthienyl)benzo[1,2-b;3,3-b] dithiophene]{3-fluoro-2[(2-ethylhexyl) carbonyl]thieno[3,4-b]thiophenediyl}) (PTB7-th) and poly[N-9′-heptadecanyl-2,7-carbazole-alt-5,5-(4′,7′-di-2-thienyl-2′,1′,3′-benzothiadiazole)] (PCDTBT), showed remarkable device performance through their broad absorption wavelength. However, their inferior charge mobility due to amorphous properties is a limiting factor for applications. In order to broaden the application of organic electronics especially for photodetectors and organic photovoltaics, new approaches, rather than synthesizing new materials, for inducing polymeric films having high charge mobility as well as wide range of absorption wavelength are highly required.

Several approaches were suggested to resolve these issues such as using additives,[14] UV irradiation,[15,16] solution aging[17] to induce polymer aggregates in solution states or thermal,[18] solvent[19] annealing in film states to increase crystallinity of polymers. In addition to such conventional approaches, meniscus-guided deposition[20–24] of polymers showed a high degree of morphological control based on directed assembly and evaporation control of polymers in solution states. However, all the approaches are mostly effective for in-plane charge transport, i.e., charge

Dr. J. Ko, Dr. Y. Kim, Prof. K. Char
The National Creative Research Initiative Center for Intelligent Hybrids
The WCU Program of Chemical Convergence for Energy
and Environment
School of Chemical and Biological Engineering
Seoul National University
Seoul 08826, Korea
E-mail: khchar@plaza.snu.ac.kr

Dr. J. S. Kang
Research Laboratory of Electronics
Massachusetts Institute of Technology
Cambridge, MA 02139, USA

Dr. R. Berger
Max Planck Institute for Polymer Research
Ackermannweg 10, D-55128 Mainz, Germany
E-mail: berger@mpip-mainz.mpg.de

Prof. H. Yoon
Department of Chemical and Biomolecular Engineering
Seoul National University of Science and Technology
Seoul 01811, Korea
E-mail: hsyoon@seoultech.ac.kr

**ADVANCED
SCIENCE NEWS**
www.advancedsciencenews.com

**ADVANCED
MATERIALS**
www.advmat.de

transport parallel to the substrate. There is a lack of versatile and effective methods to control morphology for out-of-plane charge transport, i.e., charge transport vertical to the substrate.

Anodized aluminum oxide (AAO)[25–30] or silicon[31–37] templates based nanostructuring of poly(3-hexylthiophene-2,5-diyl) (P3HT) showed enhanced charge transport along vertical direction due to an alignment of polymers provided by capillary forces and/ or their interaction with the walls of the template nanostructures. However, often high temperature or pressure is required to infiltrate polymers into nanostructures under rubbery or melted states. In addition, strong acid or base treatments are needed to remove the nanotemplate. Therefore, it is difficult to apply the Si or AAO template based nanostructuring approach to a variety of materials.

Guided self-assembly of polymers via nanostructures is a new way to control the morphology of conjugated polymers. In this study, we demonstrate a versatile approach to control the crystallinity and compatibility of conjugated polymers through the evaporation-induced self-assembly under nanoconfinement. Nanostructures are fabricated by transferring assembled films to target substrates after evaporation of solutions on polyfluoropolyether (PFPE) based nanostructures which is available at mild conditions. Increasing crystallinity as the confining sizes become smaller for semicrystalline and amorphous low bandgap polymers are demonstrated using grazing incidence X-ray diffraction (GIXD) measurements. Accordingly, they show about two magnitudes higher charge mobility along vertical direction inferred by nanoscale conductive scanning force microscopy (cSFM) and macroscale IV characteristics experiments, 0.96 cm^2 V^{-1} s^{-1} for P3HT and 0.036 cm^2 V^{-1} s^{-1} for PTB7-th.

Our novel approach is also applicable and beneficial for polymer blends which are structurally incompatible. Lots of studies have been performed to use blends of multidonor materials to use wide range of light absorption by blending low-bandgap and middle-bandgap polymers.[38–43] However, only a few combinations of polymers were available because structural and solvent compatibility between polymers is required. Blends of P3HT and PTB7-th show disrupted morphology having less crystalline structures due to their different chemical structures and chain orientation in the film states.[41–43] However, our novel approach allows to process blends regardless of their compositions. Blends of P3HT and PTB7-th are formed into compatible states, showing highly enhanced crystallinity. The nanostructured blended samples show charge mobility along out-of-plane direction about 0.73 cm^2 V^{-1} s^{-1} with a wide range of absorption wavelength from 300 to 750 nm. More importantly, our work provides a novel avenue for overcoming structural incompatibility between polymers.

Nanostructures for confined geometry were fabricated based on AAO templates. Varied feature sizes and geometries of AAO templates were fabricated by changing anodization conditions of AAO templates as shown in Figure S1 and Table S1 (Supporting Information). PFPE replica molds with hexagonal nanoholes were prepared using a two-step replication process from an AAO template; from AAO to polyurethane acrylate (PUA) as first step and from PUA to PFPE as second step. For each step, more than 20–25 replicas could be fabricated, where resulting in more than 500 duplicated PFPE replicas from single AAO template. Detailed process is described in Figure S2 (Supporting Information). Semiconducting polymers dissolved

in chloroform were self-assembled under nanoconfined geometry by spin-coating of polymer solution on nanostructured surfaces. The spin-coating process typically occurs in four steps: i) deposition, ii) spin-up, iii) spin-off, and iv) evaporation.[44,45] Centrifugal lateral forces and shear forces by air dominantly affect evaporation of solutions and final morphology of polymers in film states at the stage of spin-off and evaporation. However, in our method, centrifugal and shear forces during spin-coating process were hindered by nanostructures, which lead to slow evaporation of solvent under the nanostructures resulting preferential interaction with walls of nanostructures as shown in **Figure 1**b. Moreover, lowered vapor pressure of solvents under nanoporous media will lead to slower evaporation of solvents expected from the Kelvin equation.[46,47] Higher degree of self-assembly is expected as the diameters of nanopores become smaller due to the lowered vapor pressure of solvents under porous media. Various size and geometry of nanostructures were transferred to a target substrate after filling up the nanopores of PFPE replica molds with conjugated polymer solutions by spin-casting as shown in Figure 1a and Figure S2 (Supporting Information). Nanopillars with diameters from 40 to 170 nm, as well as nanocone structures were fabricated through this procedure as shown in Figure 1 and Figure S2 (Supporting Information). Compared to previous demanding soft lithography requiring harsh condition such as high pressure and temperature along with polymers with low glass transition or melting temperatures such as P3HT, our approach is available at low temperature (40–50 °C) and low pressure (≈4 bar) because of low surface energy properties of PFPE molds. Moreover, more than 500 replicas could be fabricated from single AAO template. The uniform size of nanostructures in large area was verified by the scanning electron microscopy (SEM) image and grazing incidence small angle X-ray scattering (GISAXS) results as shown in Figure S3 (Supporting Information).

Systematic studies on the effects of nanoconfinement on structural properties of conjugated polymers were performed by changing diameter and geometry of nanopillars. The diameter sizes of 40, 65, 90, and 170 nm nanopillars made of PCDTBT, PTB7-th, and P3HT were used for this study (Figure 1). GIXD was performed to characterize crystalline structure and orientation of polymers in nanopillars. Height of the nanopillars was fixed at 100 nm for a fair comparison in characterization of X-ray scattering and electrical properties. The aspect ratio of nanopillars has negligible effect on the morphology of polymer as shown in Figure S4 (Supporting Information) due to its limited values in the range of from 0.5 to 2.5.[35] As the degree of confinement becomes larger (diameters of nanopillars become smaller), the crystallinity of confined molecules was highly increased, which is indicated by the strong π–π staking peaks as shown in **Figure 2**a. Semicrystalline polymer (P3HT) as well as amorphous polymers (PCDTBT, PTB7-th) were strongly effected by nanoconfinement. Semicrystalline polymers, P3HT has shown dominant face-on orientation, changed from edge-on orientation, as previously reported (Figure 2d) showing about 40 times increased face-on crystalline population as shown in Figure S5 and Table S2 (Supporting Information), which were calculated from the integration of (010) peaks. In the case of amorphous low-bandgap polymer, PCDTBT and PTB7-th, their crystallinity corresponding to face-on orientation was highly
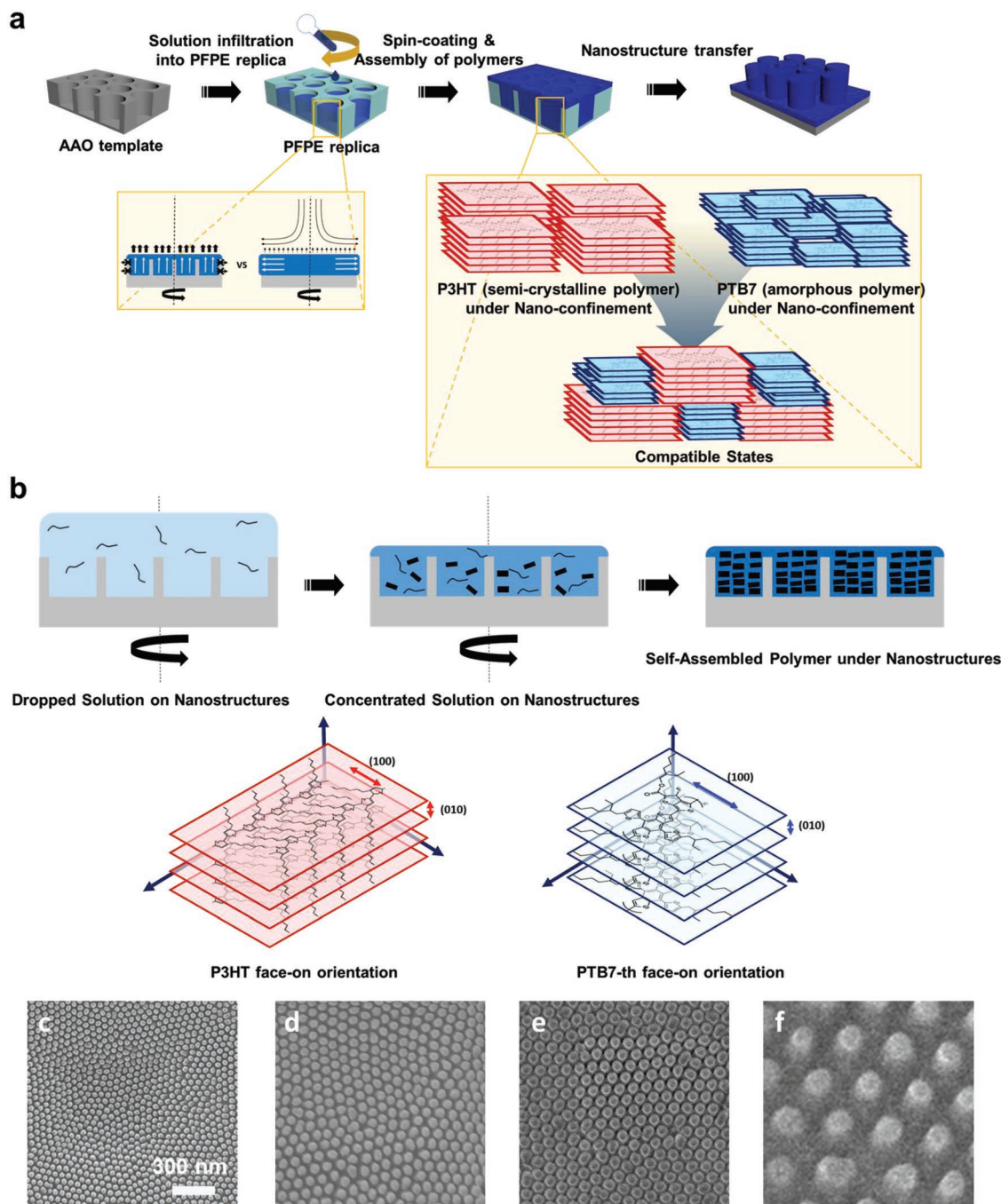
**ADVANCED
SCIENCE NEWS**

www.advancedsciencenews.com

**ADVANCED
MATERIALS**

www.advmat.de

Figure 1. a) Schematic diagram of fabricating nanostructured semiconducting polymers onto target substrates, b) assembling of polymers by spin-coating on nanostructured surfaces and resultant crystalline structures of P3HT and PTB7-th which are used in this study. c–f) SEM images of fabricated PTB7-th nanopillars having different diameters: 40, 65, 90, and 170 nm.

increased by nanoconfinement, more than eight times as shown in Figure S5 and Table S2 (Supporting Information). Moreover, PTB7-th nanocones having stronger confinement at the sharp tip part showed even more increased ratio of face-on orientation compared to that of nanopillars as explained in Figure S6 (Supporting Information), which reveals strong effects of nanoconfinement on the crystalline structures of conjugated polymers.

Significant effects of nanoconfinement on the blended semiconducting polymers were also demonstrated. It was known that blending of semicrystalline and amorphous polymers typically leads to worse structural and electrical properties than those of individual polymers because of their structural incompatibility, which originated from the different intrinsic chemical structures. Several studies have shown that adding ternary components, P3HT, more than 10% into PTB7-th/PCBM blends lead to deteriorated performance because of their different intrinsic chemical structures and chain orientation in thin film states.[41–43] This structural incompatibility between
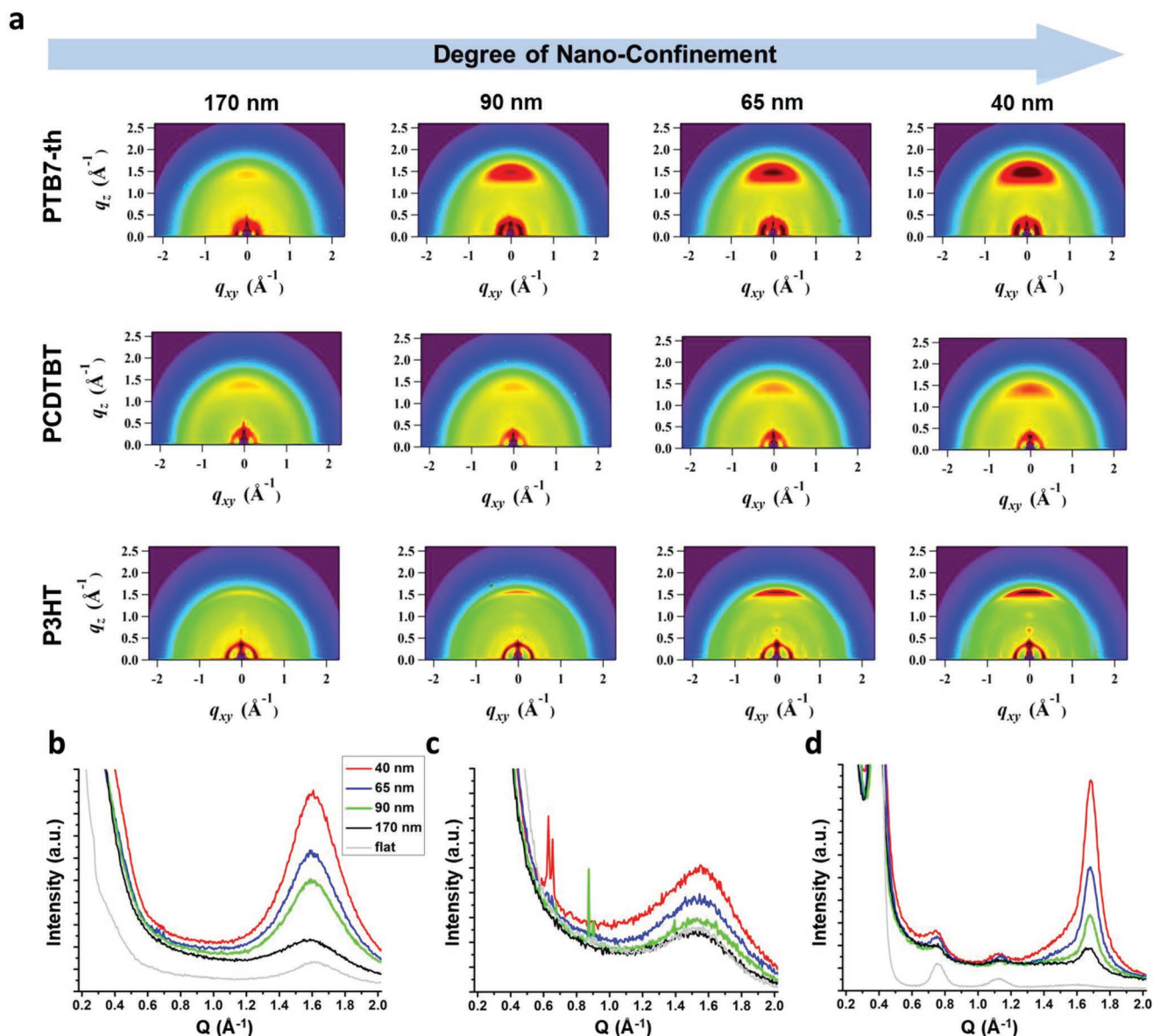
**ADVANCED
SCIENCE NEWS**
www.advancedsciencenews.com

**ADVANCED
MATERIALS**
www.advmat.de

Figure 2. a) 2D grazing-incidence X-ray diffraction (GIXD) patterns of conjugated polymers nanopillars depending on the diameter and composing polymers. b–d) 1D GIXD sptectra of PTB7-th, PCDTBT, and P3HT nanopillars along out-of-plane direction.

two polymers could be overcome by our approach. The ratio of polymers in nanostructured state was controlled by changing the ratio of the polymers in solution states. Peak positions of (010) were gradually changed as the ratio of P3HT to PTB7-th was changed from 0:10 to 10:0 as shown in Figure 3d. This result implies that the ratio of polymers in nanostructured states was successfully controlled. In addition, blends of P3HT and PTB7-th self-assembled under nanoconfinement also showed highly increased intensities of (010) peak along out-of-plane direction as shown in **Figure 3** and Figure S7 (Supporting Information). Even at 1:1 ratio of blends, more than 30 times increased intensities of (010) peaks along out-of-plane direction were observed. Moreover, that value is higher than the sum of individually confined polymers. This result demonstrates that our approach allows overcoming structural incompatibility between polymers.

To elucidate the effect of nanoconfinement on electrical properties, we measured nanoscale electrical properties of nanopillars using cSFM. The cSFM is operated in the quantitative imaging (QI) mode, where we measure the local conductance pixel-by-pixel.[48–51] The QI-mode minimizes lateral forces between the tip and the nanopillars (Figure S8, Supporting Information).[30,52,53] Thus, arrays of nanopillars with high density and aspect ratio can be measured without distortion or destruction of fragile sample features.

The conductance map of homopolymer nanopillars composed of P3HT with diameters between 40 and 170 nm displays different conductance values for individual pillars (**Figure 4**a). By defining the apex area of the nanopillars, we are able to analyze the averaged conductance values through individual pillars (Figure S9 and Table S3, Supporting Information). For
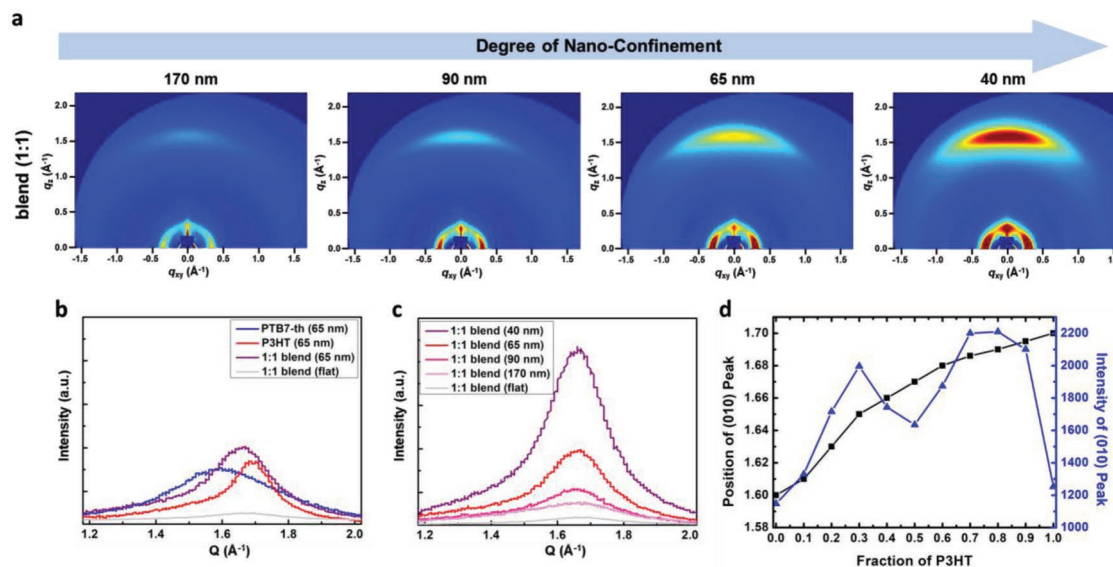
Figure 3. a) 2D grazing-incidence X-ray diffraction (GIXD) patterns of nanopillars composed of 1:1 ratio of P3HT/PTB7-th blends depending on the diameter of nanopillars. b,c) Out-of-plane line cuts to investigate effects of composing materials and diameter of nanopillars. d) Position and intensity of (010) peaks from out-of-plane direction according to fraction of composing polymers.

simplicity, we analyzed the entire conductance value for the entire scan area (Figure 4b). In particular, the highest conductance values coincide with the tip positions between the pillars. We attribute this to a higher contact area between the tip and its neighboring pillars, but the trends of peak positions of histograms correspond well with those of averaged conductance values of individual pillars (Figure 4b). The cSFM measurement revealed that the vertical conductance increases more than 50 times upon decreasing pillar diameter from 170 to 40 nm. In other words, when the degree of confinement increases the conductance through nanopillars increases as well due to an enhanced crystallinity corresponding to face-on orientation. This behavior is identical for homopolymer nanopillars composed of P3HT or PTB7-th. Nanopillars composed of blends of P3HT and PTB7-th also show significant nanoconfinement effects as expected from GIXD results. Flat samples prepared by spin-coating of blended solution showed poor conductivity which is even lower than that of amorphous PTB7-th spin-coated sample. It is noteworthy that nanoconfinement on blended samples results in a significantly enhanced average conductance which is higher than the conductance of PTB7-th nanopillars and close to that of P3HT nanopillars.

Macroscale optical and electrical properties of samples were evaluated through UV–vis spectroscopy and IV characteristics measurements. As expected from GIXD results, about 10–20% increased absorption of homopolymers by nanoconfinement along with additional enhancement in blended polymer nanopillars (Figure 4c) verify the significance of our approach. Macroscopic vertical charge mobility of nanopillars was measured using gold-coated thin PET films to have good conformal contacts with the apex of pillars following the previous methods[33,54] and explained in Figure S10 (Supporting Information). P3HT nanopillars show more than two magnitudes increased charge mobility of 0.96 cm² V⁻¹ s⁻¹. Though the infiltration of melted P3HT into nanostructured molds could lead

to higher charge mobility due to its preferential chain-on orientation as shown in Table S4 (Supporting Information), it is inapplicable to typical low-bandgap polymers which do not have glass transition temperatures and melting temperatures. It is noteworthy that our approach is versatile and widely applicable. The vertical charge mobility of PTB7-th has been increased from 2.85×10^{-4} to 0.036 cm² V⁻¹ s⁻¹ by our approach. Moreover, 1:1 blended nanopillars showed charge mobility of 0.73 cm² V⁻¹ s⁻¹ which is close to that of semicrystalline P3HT nanopillars corresponding well with GIXD and cSFM results.

In conclusion, nanoconfinements on the various conjugated polymers and their blends were demonstrated for the first time by employing our novel method. Systematic studies on the effect of nanoconfinements on structural and electrical properties of conjugated polymers show new possibilities in polymer electronics by overcoming intrinsic properties of conjugated polymers. GIXD studies on different feature sizes and geometries of conjugated polymer nanostructures show the dramatic effect of nanoconfinements on crystalline structures of polymers increasing about an order of magnitude higher population of crystallites. In addition, blends composed of structural incompatible polymers were changed into compatible states by nanoconfinements showing higher crystallinity than the sum of each components. Those significantly enhanced crystallinity and compatibility lead to more than two magnitudes higher charge mobilities supported by nanoscale cSFM measurements and macroscale IV characteristics. We expect that our concept and the results are so encouraging to stimulate new breakthrough in organic electronics based on its versatility and effectiveness.

Supporting Information

Supporting Information is available from the Wiley Online Library or from the author.
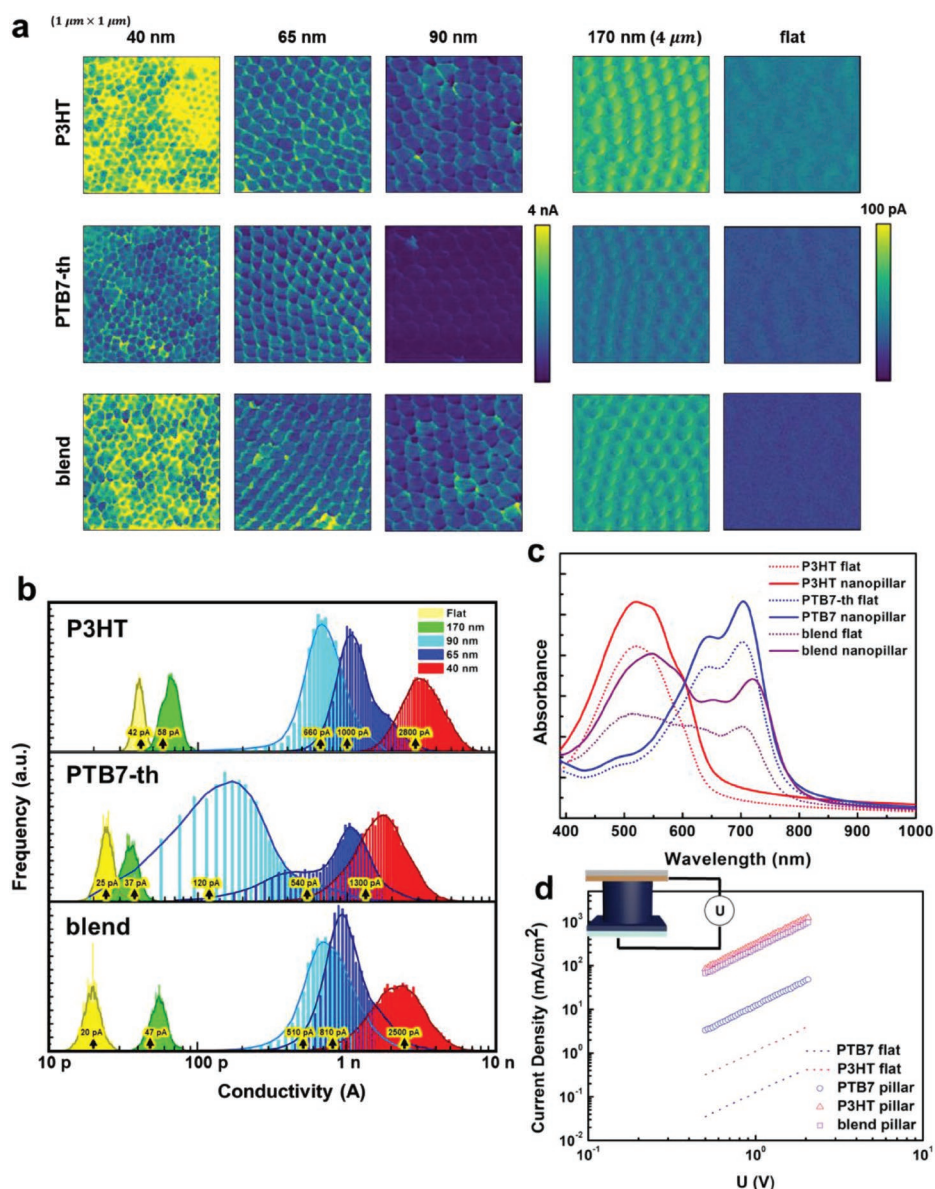
Figure 4. a) Conductive SFM images of conjugated polymer nanopillars depending on the diameter and composing materials. b) Histograms of conductance of P3HT, PTB7-th, and 1:1 blend nanopillars constructed from above cSFM images. Averaged conductivities of individual pillars from Table S3 (Supporting Information) are also included in the histograms. c) Ultraviolet–visible absorbance and d) I–V characteristics of samples depending on the composing materials.

Conflict of Interest

The authors declare no conflict of interest.

[1] Z. Bao, A. Dodabalapur, A. J. Lovinger, *Appl. Phys. Lett.* **1996**, *69*, 4108.

[2] H. Sirringhaus, N. Tessler, R. H. Friend, *Science* **1998**, *280*, 1741.

[3] H. Sirringhaus, P. J. Brown, R. H. Friend, M. M. Nielsen, K. Bechgaard, B. M. W. Langeveld-Voss, A. J. H. Spiering, R. A. J. Janssen, E. W. Meijer, P. Herwig, D. M. de Leeuw, *Nature* **1999**, *401*, 685.

[4] P. Schilinsky, C. Waldauf, C. J. Brabec, *Appl. Phys. Lett.* **2002**, *81*, 3885.

[5] Y. Li, Y. Zou, *Adv. Mater.* **2008**, *20*, 2952.

[6] J.-S. Kim, J.-H. Kim, W. Lee, H. Yu, H. J. Kim, I. Song, M. Shin, J. H. Oh, U. Jeong, T.-S. Kim, B. J. Kim, *Macromolecules* **2015**, *48*, 4339.

[7] H. Park, B. S. Ma, J.-S. Kim, Y. Kim, H. J. Kim, D. Kim, H. Yun, J. Han, F. S. Kim, T.-S. Kim, B. J. Kim, *Macromolecules* **2019**, *52*, 7721.

[8] Z. He, C. Zhong, S. Su, M. Xu, H. Wu, Y. Cao, *Nat. Photonics* **2012**, *6*, 591.

[9] S. H. Park, A. Roy, S. Beaupré, S. Cho, N. Coates, J. S. Moon, D. Moses, M. Leclerc, K. Lee, A. J. Heeger, *Nat. Photonics* **2009**, *3*, 297.

[10] Z. He, B. Xiao, F. Liu, H. Wu, Y. Yang, S. Xiao, C. Wang, T. P. Russell, Y. Cao, *Nat. Photonics* **2015**, *9*, 174.

[11] Y. Liang, Z. Xu, J. Xia, S.-T. Tsai, Y. Wu, G. Li, C. Ray, L. Yu, *Adv. Mater.* **2010**, *22*, E135.

[12] L. Dou, Y. Liu, Z. Hong, G. Li, Y. Yang, *Chem. Rev.* **2015**, *115*, 12633.

[13] N. Blouin, A. Michaud, M. Leclerc, *Adv. Mater.* **2007**, *19*, 2295.

[14] J. Peet, J. Y. Kim, N. E. Coates, W. L. Ma, D. Moses, A. J. Heeger, G. C. Bazan, *Nat. Mater.* **2007**, *6*, 497.

[15] P.-H. Chu, N. Kleinhenz, N. Persson, M. McBride, J. L. Hernandez, B. Fu, G. Zhang, E. Reichmanis, *Chem. Mater.* **2016**, *28*, 9099.

[16] G. Wang, N. Persson, P.-H. Chu, N. Kleinhenz, B. Fu, M. Chang, N. Deb, Y. Mao, H. Wang, M. A. Grover, E. Reichmanis, *ACS Nano* **2015**, *9*, 8220.

[17] N. Kleinhenz, N. Persson, Z. Xue, P. H. Chu, G. Wang, Z. Yuan, M. A. McBride, D. Choi, M. A. Grover, E. Reichmanis, *Chem. Mater.* **2016**, *28*, 3905.

[18] F. Padinger, R. S. Rittberger, N. S. Sariciftci, *Adv. Funct. Mater.* **2003**, *13*, 85.

[19] G. Li, Y. Yao, H. Yang, V. Shrotriya, G. Yang, Y. Yang, *Adv. Funct. Mater.* **2007**, *17*, 1636.

[20] Y. Diao, B. C.-K. Tee, G. Giri, J. Xu, D. H. Kim, H. A. Becerril, R. M. Stoltenberg, T. H. Lee, G. Xue, S. C. B. Mannsfeld, Z. Bao, *Nat. Mater.* **2013**, *12*, 665.

[21] Y. Diao, Y. Zhou, T. Kurosawa, L. Shaw, C. Wang, S. Park, Y. Guo, J. A. Reinspach, K. Gu, X. Gu, B. C. K. Tee, C. Pang, H. Yan, D. Zhao, M. F. Toney, S. C. B. Mannsfeld, Z. Bao, *Nat. Commun.* **2015**, *6*, 7955.

[22] X. Gu, L. Shaw, K. Gu, M. F. Toney, Z. Bao, *Nat. Commun.* **2018**, *9*, 534.

[23] S. Schott, E. Gann, L. Thomsen, S.-H. Jung, J.-K. Lee, C. R. McNeill, H. Sirringhaus, *Adv. Mater.* **2015**, *27*, 7356.

[24] L. Shaw, P. Hayoz, Y. Diao, J. A. Reinspach, J. W. F. To, M. F. Toney, R. T. Weitz, Z. Bao, *ACS Appl. Mater. Interfaces* **2016**, *8*, 9285.

[25] G. Ding, C. Li, X. Li, Y. Wu, J. Liu, Y. Li, Z. Hu, Y. Li, *Nanoscale* **2015**, *7*, 11024.

[26] T. Pfadler, M. Coric, C. M. Palumbiny, A. C. Jakowetz, K.-P. Strunk, J. A. Dorman, P. Ehrenreich, C. Wang, A. Hexemer, R.-Q. Png, P. K. H. Ho, P. Müller-Buschbaum, J. Weickert, L. Schmidt-Mende, *ACS Nano* **2014**, *8*, 12397.

[27] T. Kim, H. Yoon, H.-J. Song, N. Haberkorn, Y. Cho, S. H. Sung, C. H. Lee, K. Char, P. Theato, *Macromol. Rapid Commun.* **2012**, *33*, 2035.

[28] J. S. Kim, Y. Park, D. Y. Lee, J. H. Lee, J. H. Park, J. K. Kim, K. Cho, *Adv. Funct. Mater.* **2010**, *20*, 540.

[29] D. Chen, W. Zhao, T. P. Russell, *ACS Nano* **2012**, *6*, 1479.

[30] J. Ko, J. Song, H. Yoon, T. Kim, C. Lee, R. Berger, K. Char, *Adv. Mater. Interfaces* **2016**, *3*, 1600264.

[31] X. Lu, H. Hlaing, C.-Y. Nam, K. G. Yager, C. T. Black, B. M. Ocko, *Chem. Mater.* **2015**, *27*, 60.

[32] X. He, F. Gao, G. Tu, D. Hasko, S. Hüttner, U. Steiner, N. C. Greenham, R. H. Friend, W. T. S. Huck, *Nano Lett.* **2010**, *10*, 1302.

[33] V. Skrypnychuk, G.-J. A. H. Wetzelaer, P. I. Gordiichuk, S. C. B. Mannsfeld, A. Herrmann, M. F. Toney, D. R. Barbero, *Adv. Mater.* **2016**, *28*, 2359.

[34] Y. Yang, K. Mielczarek, M. Aryal, A. Zakhidov, W. Hu, *Nanoscale* **2014**, *6*, 7576.

[35] D. E. Johnston, K. G. Yager, H. Hlaing, X. Lu, B. M. Ocko, C. T. Black, *ACS Nano* **2014**, *8*, 243.

[36] G. Ding, K. Wang, X. Li, C. Wang, Z. Hu, J. Liu, *Polym. Chem.* **2017**, *8*, 2666.

[37] M. Aryal, K. Trivedi, W. W. Hu, *ACS Nano* **2009**, *3*, 3085.

[38] J. Lee, S. M. Lee, S. Chen, T. Kumari, S.-H. Kang, Y. Cho, C. Yang, *Adv. Mater.* **2018**, e1804762.

[39] Y. (M.) Yang, W. Chen, L. Dou, W.-H. Chang, H.-S. Duan, B. Bob, G. Li, Y. Yang, *Nat. Photonics* **2015**, *9*, 190.

[40] Y. Zhang, D. Deng, K. Lu, J. Zhang, B. Xia, Y. Zhao, J. Fang, Z. Wei, *Adv. Mater.* **2015**, *27*, 1071.

[41] Y. Ohori, S. Fujii, H. Kataura, Y. Nishioka, *Jpn. J. Appl. Phys.* **2015**, *54*, 04DK09.

[42] H. Huang, L. Yang, B. Sharma, *J. Mater. Chem. A* **2017**, *5*, 11501.

[43] T. Goh, J.-S. Huang, B. Bartolome, M. Y. Sfeir, M. Vaisman, M. L. Lee, A. D. Taylor, *J. Mater. Chem. A* **2015**, *3*, 18611.

[44] N. Sahu, B. Parija, S. Panigrahi, *Indian J. Phys.* **2009**, *83*, 493.

[45] J. Y. Na, B. Kang, S. G. Lee, K. Cho, Y. D. Park, *ACS Appl. Mater. Interfaces* **2017**, *9*, 9871.

[46] S.-W. Cho, C.-K. Kim, J.-K. Lee, S. H. Moon, H. Chae, *J. Vac. Sci. Technol., A* **2012**, *30*, 051301.

[47] H. Lee, J.-H. Kim, G. Wu, H.-M. Lee, J. Kim, D. Kwon, S. Yang, C.-K. Kim, H. Yoon, *Adv. Mater. Interfaces* **2018**, *5*, 1801142.

[48] S. A. L. Weber, N. Haberkorn, P. Theato, R. Berger, *Nano Lett.* **2010**, *10*, 1194.

[49] R. Berger, A. L. Domanski, S. A. L. Weber, *Eur. Polym. J.* **2013**, *49*, 1907.

[50] A. Klasen, P. Baumli, Q. Sheng, E. Johannes, S. A. Bretschneider, I. M. Hermes, V. W. Bergmann, C. Gort, A. Axt, S. A. L. Weber, H. Kim, H.-J. Butt, W. Tremel, R. Berger, *J. Phys. Chem. C* **2019**, *123*, 13458.

[51] R. Berger, B. Grévin, P. Leclère, Y. Zhang, *Beilstein J. Nanotechnol.* **2019**, *10*, 132.

[52] T. J. H. Haschke, *Laser Focus World* **2012**, *48*, 25.

[53] Y. Aoyama, O. Douhéret, P. Leclère, D. Moerman, J. Mizukado, H. Suda, R. Lazzaroni, Y. Yoshida, *Org. Electron.* **2017**, *43*, 142.

[54] D. R. Barbero, N. Boulanger, *ACS Nano* **2017**, *11*, 9906.